Time-resolved optical tomography using short-pulse laser for tumor detection

Gopalendu Pal, Soumyadipta Basu, Kunal Mitra, and Tuan Vo-Dinh

Our objective is to perform a comprehensive experimental and numerical analysis of the short-pulse laser interaction with a tissue medium with the goal of tumor–cancer diagnostics. For a short-pulse laser source, the shape of the output signal is a function of the optical properties of the medium, and hence the scattered temporal optical signal helps in understanding the medium characteristics. Initially experiments are performed on tissue phantoms embedded with inhomogeneities to optimize the time-resolved optical detection scheme. Both the temporal and the spatial profiles of the scattered reflected and transmitted optical signals are compared with the numerical modeling results obtained by solving the transient radiative transport equation using the discrete ordinates technique. Next experiments are performed on *in vitro* rat tissue samples to characterize the interaction of light with skin layers and to validate the time-varying optical signatures with the numerical model. The numerical modeling results and the experimental measurements are in excellent agreement for the different parameters studied. The final step is to perform *in vivo* imaging of anesthetized rats with tumor-promoting agents injected inside skin tissues and of an anesthetized mouse with mammary tumors to demonstrate the feasibility of the technique for detecting tumors in an animal model.

OCIS codes: 140.0140, 170.0170, 170.3660, 170.6920.

1. Introduction

The use of light for the probing and imaging of biological tissue media offers the promise for safe, noninvasive, and inexpensive clinical imaging modalities with diagnostic ability. The detection of early neoplastic changes is important from an outcome viewpoint, since once invasive carcinoma and metastases have occurred, treatment is difficult. At present, excisional biopsy followed by histology is considered to be one of the "gold standards" for the diagnosis of early neoplastic changes and carcinoma. In some cases, cytology rather than excisional biopsy is performed. These techniques are powerful diagnostic tools because they provide high-resolution spatial and morphological information of the cellular and subcellular structures of tissues. The use of staining and processing can enhance contrast and specificity of histopathology. However, both of these diagnostic procedures require the physical removal of specimens followed by tissue processing in the laboratory. As such, these procedures incur a relatively high cost because specimen handling is required, and more importantly diagnostic information is not available in real time. Moreover, in the context of detecting early neoplastic changes, both excisional biopsy and cytology can have unacceptable false negative rates often arising from sampling errors. Therefore optical imaging techniques have gained popularity for medical diagnostics.

Currently used optical diagnostic technologies can be broadly classified into two categories: namely, point measurement for spectroscopic diagnostics and optical imaging, often referred to as optical tomography aimed at recording a 2D or 3D image of an area or volume of the sample of interest. Spectroscopic diagnostics all share the common feature that they measure some spectroscopic properties that are related to the molecular composition and structure of biochemical species in the tissue of interest. There are several spectroscopic methods that are used for optical diagnostics: fluorescence, elastic scattering, Raman (inelastic scattering), infrared absorption, etc. For example, a number of investigators have investigated point-detection methods such as laser-induced fluorescence (LIF) to discriminate tumors

G. Pal, S. Basu, and K. Mitra (kmitra@fit.edu) are with the Mechanical and Aerospace Engineering Department, Florida Institute of Technology, 150 West University Boulevard, Melbourne, Florida 32901-0000. T. Vo-Dinh (vodinht@oml.gov) is with the Oak Ridge National Laboratory, P. O. Box 2008, Mail Stop 6101, Oak Ridge, Tennessee 37831-6101.

Received 4 November 2005; revised 8 February 2006; accepted 7 March 2006; posted 24 March 2006 (Doc. ID 65751).

0003-6935/06/246270-13$15.00/0

from normal tissues.[1–11] Various aspects of LIF techniques in imaging and point-measurement systems for cancer diagnosis have been recently reviewed.[12]

The potential of optical tomography as a new diagnostic tool has stimulated considerable interest since the past decade.[13–19] Although limited to about the first 5 cm of the body, the technique offers several advantages often not available in established imaging modalities such as ultrasound, x-ray computed tomography, and magnetic resonance imaging (MRI).[20–22] Two basic measurement methodologies are used for imaging: (i) frequency-domain methods that employ harmonically modulated photon density waves and phase-resolved detection, which measure the phase shift of the photon density waves and (ii) time-domain methods that use pulsed excitation and ultrafast detectors to examine the response of tissue to a short pulse of incident light. For frequency-domain measurements, most experimental work performed so far has utilized frequencies of a few hundred megahertz, which is equivalent to a temporal resolution of a few nanoseconds, and photon density wavelengths of the order of a meter.[23–25] It has been reported in the literature that there is a need for high-modulation frequencies to obtain images with high resolution when imaging tissues having particularly low-average absorption and high-scattering coefficients.[26]

Time-domain optical imaging using short-pulse lasers has developed as a powerful tool in medical diagnostics. This technique presents several advantages over other conventional cw imaging techniques. Short-pulse laser probing techniques for diagnostics have distinct advantages over very large pulse width or continuous wave lasers primarily due to the additional information conveyed by the temporal distribution of the observed signal.[15,16,27,28] The distinct feature is the multiple-scattering-induced temporal distributions, which persists for a time period greater than the duration of the source pulse and is a function of the source pulse width as well as the optical properties of the medium. If the detection is carried out at the same short time scale (comparable to the order of the pulse width), the signal continues to be observed even for long times after the pulse has been off due to the time taken for the photons to migrate to the detector after multiple scattering in the media. Therefore detectors with high-temporal resolution are required to collect the scattered reflected and transmitted photons.

Time-domain optical imaging can again be broadly classified into two types, namely, time-gating and time-resolved measurements. A time-gated technique uses the ballistic photons for image reconstruction.[29–33] Experiments have demonstrated that measurements of the earliest arriving photons, which have traveled the shortest paths between the source and the detector, can be used to generate images with significantly improved spatial resolution. However, the scarcity of photons with the shortest path lengths especially for optically thick tissue media limits the spatial resolution that the time-gating method is able to achieve.[34]

To overcome the scarcity of photons in time-gating, time-resolved measurements that use a diffuse component of the photons for image reconstruction have been used by many groups.[15,16,31,35–40] Time-resolved techniques improve the localization and characterization of the inhomogeneities as information on the path length of each photon becomes available. Inhomogeneities differing from the surrounding tissue in terms of optical properties have a different influence on the distribution of the times of flight of photons. The temporal shape of the measured optical signals provides detailed information about medium characteristics including the presence of inhomogeneities and tumors.

To predict the optical properties of tissues from time-resolved scattered optical signal measurements, the development of an inverse algorithm is required. Before the development of complex inverse algorithms, accurate forward solutions of a transient radiative transport equation necessary to analyze short-pulse laser propagation through tissues are critical. In the most previous analysis, the transient term of the radiative transport equation (RTE) is usually neglected. The simulation of the transient radiation transport process is more complicated than the traditional steady-state analysis due to the hyperbolic wave nature of the equation coupled with the in-scattering integral term making it an integrodifferential equation.[27,28] Diffusion approximation has been commonly used in the literature for solving the transient RTE for analyzing short-pulse laser propagation through tissue media.[27,31,41,42] But time-resolved experiments on tissues have shown that diffusion-based analyses are accurate for thick samples but fail to match experimental data for sample thicknesses comparable to the mean free path.[29] Monte Carlo simulation results are found to match the experimental measurements on tissue phantoms, but diffusion theory failed to accurately predict the scattering coefficient.[43] A detailed discussion of the validity of the diffusion in bio-optical imaging is also provided in the literature, and it has been pointed out that diffusion approximations have a limitation that should not be ignored.[44] Recently more accurate solutions of transient RTE have been obtained using other techniques such as the discrete ordinates method (DOM),[45–47] Monte Carlo simulation,[48,49] reverse Monte Carlo solution,[50] integral transfer technique,[51,52] radiation element method,[53] and the discrete transfer method.[54] Only a few studies have been devoted to multidimensional problems such as a diffusion-based 3D model[55] and for phantoms containing inhomogeneities such as using time-of-flight measurements.[18] Among all the methods, DOM is computationally inexpensive and is memory efficient as compared to the other numerical schemes. It offers the best compromise between accuracy and computational time. There is no restriction on the optical thickness and scattering albedo variations while using DOM. Most of these previous

studies have not compared the numerical modeling results with the experimental measurements.

To compare the experimental measurements with the numerical modeling results, there is a need to develop accurate solutions for the transient radiative transport equation in 2D and 3D geometry. Very few studies have been reported in the literature regarding the validation of experimental measurements with that obtained from the numerical models. Besides the model validation of experimental measurements for most of the previous work has been primarily restricted to homogenous samples.[36,56,57] Moreover, validation of experimental measurements for tissue phantoms containing inhomogeneities reported in the literature has been performed using a diffusion-based model.[16,34,58] Authors of this group have validated the experimental measurements of transmitted signals for tissue phantoms with inhomogeneities embedded in them with solutions of the RTE obtained using DOM.[40] More studies are necessary for the validation of the forward model of the RTE with experimental measurements for the determination of tissue optical properties. Moreover, the measurement of the transmitted optical signals is not practical for imaging internal organs such as the brain, the lungs, the kidneys, etc. for cancer–tumor detection. Hence there is a need for the measurement and validation of both the reflected and the transmitted scattered optical signals from a tissue phantom containing inhomogeneities.

Small animal imaging systems have received increasing attention over the past decade. The interest is motivated by advances in animal models of human diseases, and the possibility to noninvasively monitor the progression of diseases in living small animals. Different imaging techniques such as confocal imaging,[59] single-photon emission tomography,[60] MRI imaging,[61,62] fluorescence imaging,[63] and cw optical tomography[62] have been used for the detection of tumors in small animals. However, very few studies have been reported on time-domain optical imaging of animals. The goal of this paper will be to demonstrate the feasibility of using the time-resolved optical tomography system using a short-pulse laser for the detection of tumors in mice and rats.

A fiber-optic system is used for the laser incidence as well as for the collection of scattered reflected and transmitted optical signals from the samples. The fiber-optic probe assembly mounted on a three-axis translation stage is used to scan any tissue area and is connected to a computerized data acquisition system. The measured optical signals from the scanned area are directly fed into National Instrument's LABVIEW 7.1 software to view the 3D distribution of the intensity distribution in real time. The advantages of using a fiber-optic approach are the high-transmission efficiency of fiber optics, and the fact that light can easily be transmitted to remote locations for imaging of internal organs inside the body.

In this paper, the first experimental measurements of both the scattered reflected and the transmitted signals are validated with the numerical modeling results obtained by solving the RTE using the DOM for tissue phantoms containing inhomogeneities. Experiments are next performed on freshly excised rat tissue samples, and the measured reflected optical signal measurements are also validated with the numerical modeling results. To the best of our knowledge, this would be the first time that experimental validation of the optical signal measurements using numerical models has been performed on animal tissue samples. Experiments are finally performed on anesthetized rats with tumor-promoting agents applied on the skin, as well as injected below the skin surface, and also on anesthetized mice with mammary tumors to analyze their effect on optical signals. The goal is to demonstrate the feasibility of using a time-resolved optical tomography system for the detection of tumors in an animal model.

2. Sample Preparation

Initial experiments are performed to study the interaction of a short-pulse laser with tissue phantoms for the detection of inhomogeneities with the aim of optimizing the time-resolved optical tomography detection scheme. Experiments are next performed on freshly excised mouse and rat tissue samples to characterize the tissue response to a short-pulse laser source. Finally, experiments are performed on the anesthetized rats having mammary tumors and as well as tumor-promoting agents injected on and below the skin surface to demonstrate the feasibility of using a time-resolved optical tomography system for the detection of tumors in an animal model.

A. Tissue Phantom Preparation

A typical tissue phantom used in this study as shown in Fig. 1 has dimensions of 50 mm (width, W) $\times$ 25 mm (height, H) $\times$ 8 mm (thickness, L). The tissue phantoms are made of an Araldite 502 embedding medium. Araldite 502 resin is polymerized with dodecenyl succinic anhydride (DDSA) and catalyzed with 2,4,6-tri phenol (DMP-30) in the volumetric ratio of 1:0.85:0.04. The samples are cured overnight at 35 °C, the next day at 45 °C, then again overnight at 60 °C. The refractive index of the resin is 1.54. Titanium dioxide (TiO_2) having a mean diameter = 0.3 μm is added as a scatterer to the resin base and India ink is used as an absorber. The scattering and absorption coefficients are varied by varying the concentration of the TiO_2 and India ink in the resin matrix.[40,64] The tissue phantoms are cast in aluminum molds. The tissue phantom has a strong adhesion property to aluminum as well as to other metals. Silicon-based mold release agents with crytox are sprayed on the molds before the phantom is cast, which facilitates the easy removal of the samples after they are cast.

Inhomogeneities typically of a 4 mm diameter are drilled in the center of the samples. For some experiments, inhomogeneities are drilled off axis away from the center. The drilled holes are filled with different scattering coefficients other than the base tissue matrix and again cured in the oven for a day.

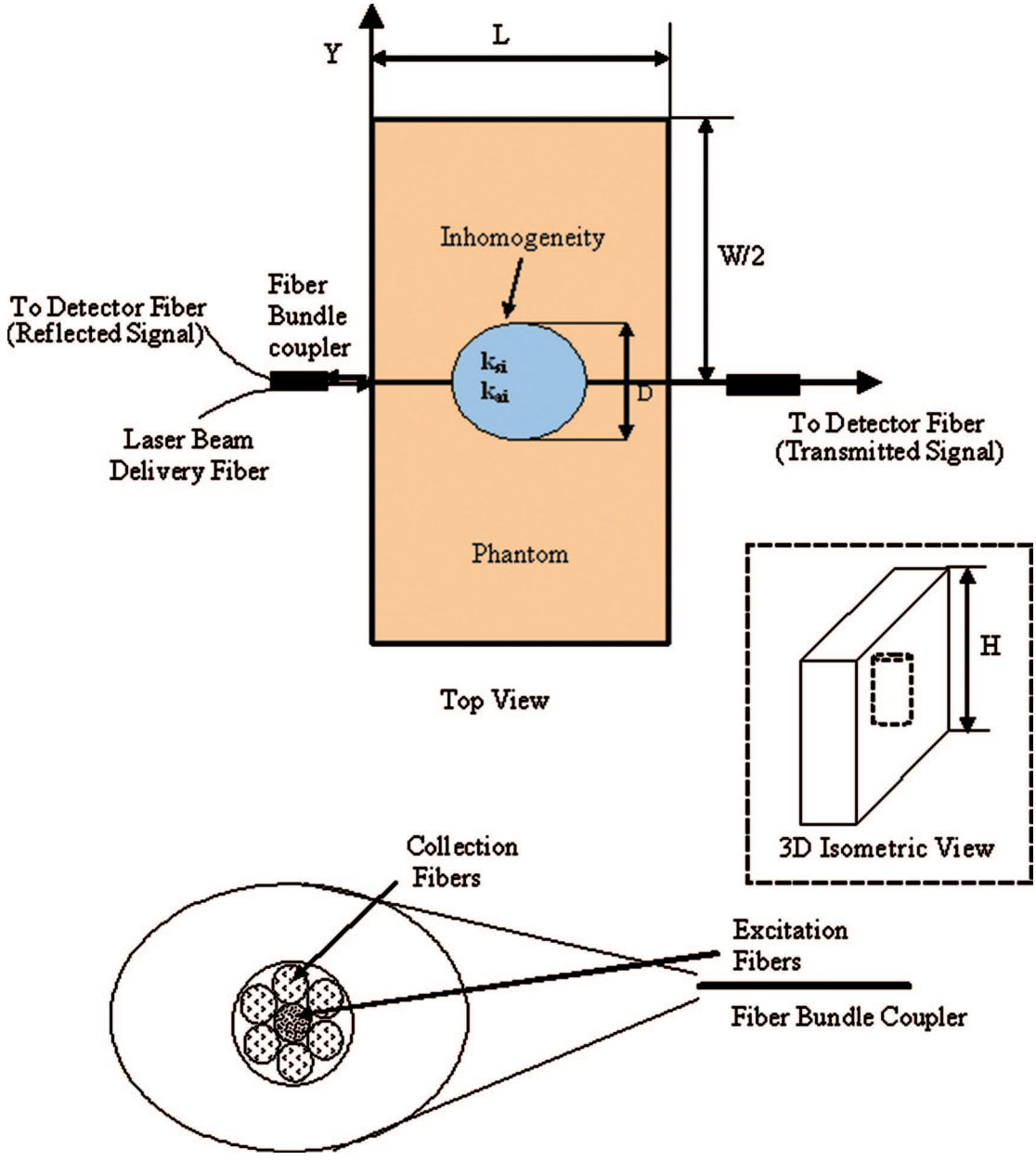

Fig. 1. (Color online) Schematic of a tissue phantom containing the inhomogeneity used for experiments.

B. Animal Tissue Preparation

Freshly excised rat tissue samples are obtained from the Wistar rat of the Alvino trait. Tissue samples are cut in such a way that either skin or skin and muscle combined are obtained to study the effect of different layers. The rat skin layers are typically 3 mm thick, while the tissue samples with combined skin and muscle layers are typically 8 mm thick. A typical cross section of the tissue samples used is 30 mm $\times$ 20 mm.

C. Injection of Tumor-Promoting Agents in Rats

Experiments are next performed on an anesthetized rat with tumor-promoting agents injected on the skin surface as well as below the skin surface. Studies are performed on rats that are anesthetized with ketamine hydrochloride (Ketaset, Ft. Dodge Laboratories, Ft. Dodge, Iowa), administered intraperitoneally at 150 mg/kg. The tumor diameter is around 2 mm. For the case of tumor-promoting agents injected below the surface, the depth at which the tumor is injected is unknown, and the goal is to detect the location and depth of the tumor using time-resolved measurement techniques. The animals are kept under controlled conditions of temperature and humidity. After the completion of the experiments, the rats are allowed to recover from the effects of the anesthesia before being introduced to the animal colony.

D. Mice with Mammary Tumors

Mice used in this study, strain FVB/N-Tg(MMTV-neu)202Mul/J, are purchased from the Jackson Lab-

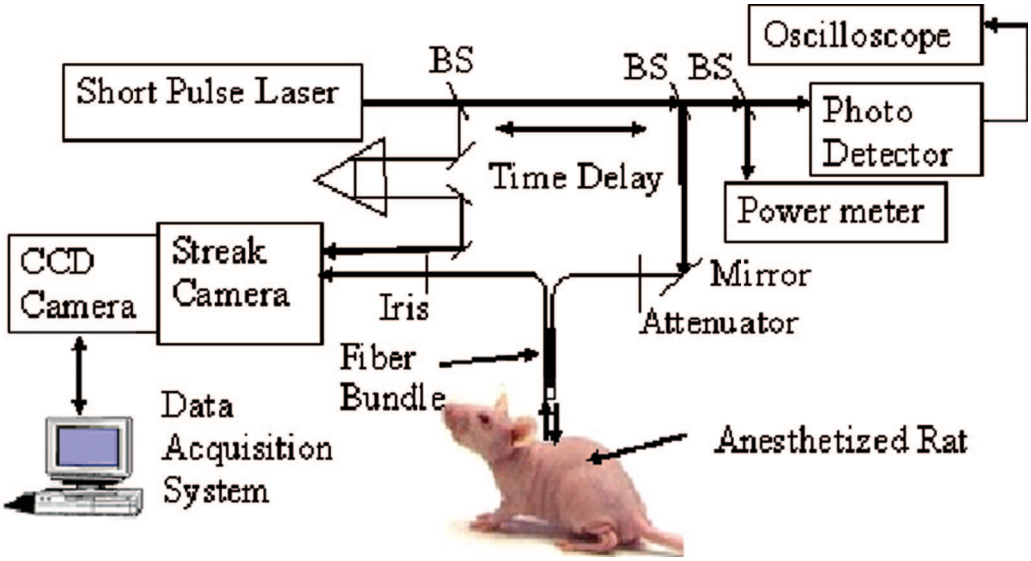

Fig. 2. (Color online) Schematic of an experimental setup for the measurement of a reflected signal.

oratory, Bar Harbor, Maine. These mice contain the mouse mammary tumor virus (MMTVneu) transgene, expressed in the mammary tissues, salivary glands, and lungs. Mice are purchased as retired breeders containing focal metastatic tumors in the mammary glands. The mice are anesthetized in the same way as the rats mentioned in Subsection 2.C. Animals are allowed to fully recover before being reintroduced to the animal colony; no signs of stress have been observed before, during, or after the experimental procedures. All animal experimental procedures are approved by Florida Tech's Institutional Animal Care and Use Committee.

3. Experimental Setup

The schematic of the experimental setup for the measurement of the scattered reflected optical signals for the case of the imaging of rats with mammary tumors is shown in Fig. 2. The schematic of the setup for the measurements of the transmitted optical signal is not presented here and can be found in the literature.[40]

A mode-locked short-pulse laser operating at a wavelength of 514 nm with a temporal pulse width (t_p) of 200 ps, and a repetition rate of 76 MHz is used for the study. The laser beam is first incident on a plate-type beam splitter. The first beam splitter divides the emitted laser beam into two parts in the ratio of 9:1. The part having 10% of the main laser beam is passed through a delay generating prism and is fed into the Hamamatsu streak camera unit (C 1587) for observing the raw pulse as a reference. A second beam splitter further splits the beam with 90% of the main laser beam energy into two parts again in the ratio of 9:1. The beam with 90% energy of the split beam is focused onto the excitation end of a fiber-optic probe and is then transmitted to the distal end where it illuminates the samples. The beam with 10% energy of the split beam is further split by a third beam splitter in the ratio of 9:1. The beam with 90% energy of the split beam is used to monitor the pulse width of the incident beam using an 18.5 ps ultrafast photodetector (New-focus, Model 1954). The output of the detector is measured on the Tektronix (7854) oscilloscope with sampling modules. The beam with 10% of the energy of the split beam is used to monitor the power of the laser beam incident on the sample using appropriate calibration.

To feed the laser light into the fibers for the precise and efficient delivery of light to the samples, various focusing elements such as lenses, mirrors, and collimators are used. The scattered reflected and transmitted optical signals from the samples collected using the fiber-optic probe is fed into the same Hamamatsu streak camera. A fiber-optic source detector bundle assembly, as shown in Fig. 1, is used for the experiments. In this fiber-optic assembly, the fiber at the center acts as the source to deliver the laser light to the desired region and the fibers around the source fiber are used as collectors to capture the reflected or the transmitted signals from the sample. The probe assembly is mounted on a three-axis vertical translation stage. The average power incident on the sample is of the order of 12–15 mW. Hence attenuators are used to reduce the incident power on the samples as required so as not to saturate the streak camera. The fiber used in the study is a 1 m long multimode fiber with a core diameter of 62.4 μm and an outer diameter of 125 μm, a numerical aperture of 0.21, and a V number of 222.314. The beam attenuation inside the fiber is 5 dB/km. The fibers have Franck–Condon (FC) connectors at both ends. The typical insertion loss of the FC connector is around 0.3 dB.

4. Numerical Modeling

In this paper, the tissue medium is approximated by an anisotropically scattering and absorbing rectangular enclosure in which an inhomogeneity is embed-

ded (see Fig. 1). The transient radiative transfer equation is used to analyze short-pulse laser propagation through tissues and is given by[28,45]

$$\frac{1}{c}\frac{\partial I(x, y, \Omega, t)}{\partial t} + \mu\frac{\partial I(x, y, \Omega, t)}{\partial x} + \eta\frac{\partial I(x, y, \Omega, t)}{\partial y} + k_e I(x, y, \Omega, t) = \frac{k_s}{4\pi}\int_{4\pi}\Phi(\Omega', \Omega) I(x, y, \Omega', t)\mathrm{d}\Omega' + S(x, y, \Omega, t), \quad (1)$$

where I is the scattered diffuse intensity (W m^{-2} sr^{-1}), k_e and k_s are the extinction coefficient and the scattering coefficient, respectively, Φ is the phase function, Ω is the solid angle, c is the velocity of light in the medium, x and y are the spatial coordinates, t is the time, and S is the source term. The pulsed radiation incident on the tissue medium (see Fig. 1) is a Gaussian pulse having a temporal duration (pulse width) t_p at FWHM. The total intensity can be separated into a collimated component, corresponding to the incident source pulse and a scattered intensity I as described by Eq. (1). The source function S in Eq. (1) is due to the collimated component of the irradiation.

Numerical results have been obtained by solving Eq. (1) using the discrete ordinate method as described in detail in the Mitra and Kumar[45] previous papers of and Sakami *et al.*[46] and is not repeated here. The computational time is about 180 s on a LINUX workstation with a 3.2 GHz CPU for 80 discrete ordinates quadratures. Spatial grid size of 0.5 mm and temporal grid size of 0.5 ps are used in the simulations. The accuracy of the numerical results is validated by ensuring that the results are independent of the grid sizes. The sample height is very large compared to the beam diameter, and hence, a 2D transient radiative transfer model is applied. Results obtained using numerical simulations are compared with the corresponding reflected and transmitted optical signals measured experimentally.

5. Results and Discussion

Experiments are first performed on homogeneous tissue phantoms and tissue phantoms containing inhomogeneities to optimize the time-resolved optical tomography system. Scattered optical reflected and transmitted signal measurements are validated with the numerical modeling results. Next, experiments are performed on *in vitro* tissue samples to characterize the optical signatures from real tissues and to compare the experimental measurements with the numerical modeling results. Finally, *in vivo* experiments are performed in live anesthetized rats with tumor-promoting agents applied on the skin surface and injected below the skin surface and as well as in live anesthetized mouse with mammary tumors to demonstrate the feasibility of using this technique for tumor detection in an animal model.

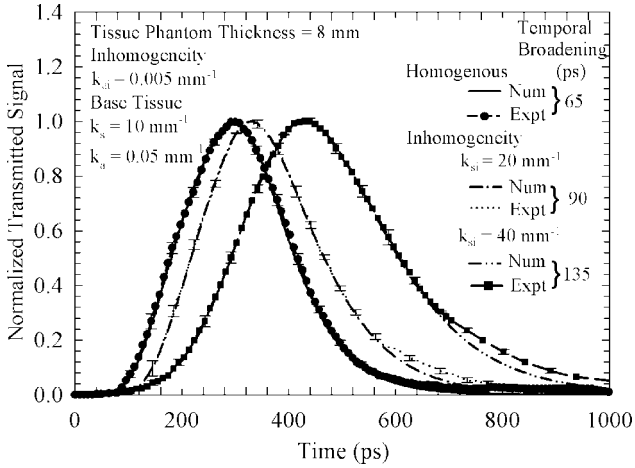

Fig. 3. Effect of variation of the scattering coefficient of an embedded inhomogeneity on temporal transmitted signals for tissue phantoms containing an inhomogeneity.

A. Experiments with Tissue Phantoms and Numerical Model Validation

In Fig. 3, the normalized transmitted signals are compared between a homogenous tissue phantom and that of a phantom containing an inhomogeneity at the center having different scattering coefficients. For the homogenous tissue phantom, the values of the scattering coefficient (k_s) and the absorption coefficient (k_a) used are 10 and 0.05 mm^{-1}, respectively.[65] The thickness (L) of the tissue phantoms for all the cases is 8 mm. For the tissue phantom containing inhomogeneity, the optical properties of the base tissue phantom is the same as that for the homogenous phantom while two different values of scattering coefficients of the inhomogeneity (k_{si}) are used: 20 and 40 mm^{-1}. The absorption coefficient of the inhomogeneity (k_{ai}) is equal to 0.005 mm^{-1}. There is very good agreement between the numerical modeling results and the experimental measurements with a little separation in the tail section. This separation can be attributed to the fact that as the scattering coefficient is increased, the photons suffer random scattering and persist inside the medium for a longer time resulting in very few photons leaving the medium. However, since in this technique the amplitude and the pulse width at the FWHM are most important, the mismatch between the experimental measurements and the numerical results at the tail of the pulse does not produce a significant loss of information regarding the tissue interior. It is observed that with the increase in the scattering coefficient of the inhomogeneity, the temporal broadening of the output transmitted pulse (t_{bp}) increases. A higher-scattering coefficient increases the optical depth of the medium, and as a result, the transmitted photons take a longer time to reach the detector that is manifested in the higher temporal broadening of the transmitted optical signal. Figure 4 shows the comparison of the normalized reflected signals between a homogenous tissue phantom and the tissue phantom containing an inhomoegneity at the center for differ-

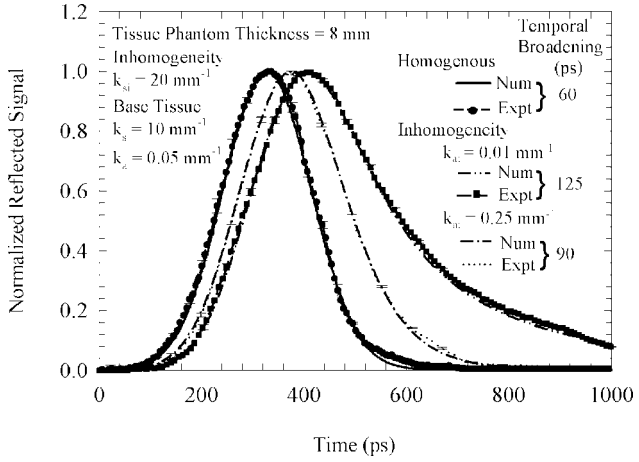

Fig. 4. Effect of variation of the absorption coefficient of an embedded inhomogeneity on temporal reflected signals for tissue phantoms containing an inhomogeneity.

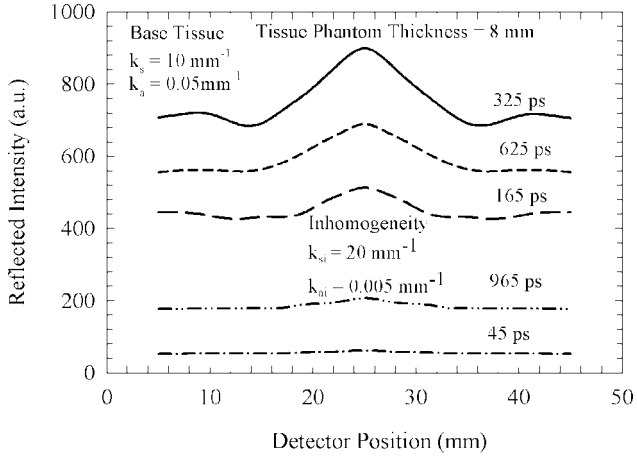

Fig. 6. Spatial reflected intensity distributions for a tissue phantom containing an inhomogeneity at different time instants.

ent absorption coefficients of the inhomogeneity. The scattering coefficient of the inhomogeneity is kept constant at 20 mm^{-1}, while two different values of absorption coefficients of the inhomogeneities are used: 0.25 and 0.01 mm^{-1}. With the increase in the absorption coefficient of the inhomogeneity, a greater number of photons is absorbed within the medium. This results in a greater attenuation of the incident light, and as a result, the total temporal broadening of the reflected pulse reduces with an increase in the absorption coefficient. For both Figs. 3 and 4, there is also a change in the magnitude of the intensity values, but this effect is masked due to the normalization of the signals.

Figures 5 and 6 show the spatial transmitted and reflected intensity distributions for the tissue phantom containing an inhomogeneity at different times. It is observed that for very long and for very short times, the transmitted and reflected signals do not provide the contrast for the inhomogeneity location. For long times, a majority of the photons are lost, while for shorter times, very few photons reach the detector. The optical signals measured very close to the edge of the phantom showed fluctuations due to the boundary effects, and hence are not considered. At the time instant of approximately 325 ps, the distinction between the inhomogeneity location and the surrounding base tissue is best observed. Therefore a selection of an appropriate time window is critical for the maximum contrast between the tissue phantom and the inhomogeneity. Figure 7 shows the comparison between the numerical modeling results and the experimentally measured transmitted and reflected signals for the best time instant of 325 ps as presented in Figs. 5 and 6. A very good match is observed between the experimental measurements and the numerical modeling results. The transmitted and reflected signals show an opposite trend. While the reflected intensity is highest at the location of the inhomogeneity, the transmitted intensity is lowest at that location. Since the inhomogeneity has a higher scattering coefficient compared to the surrounding

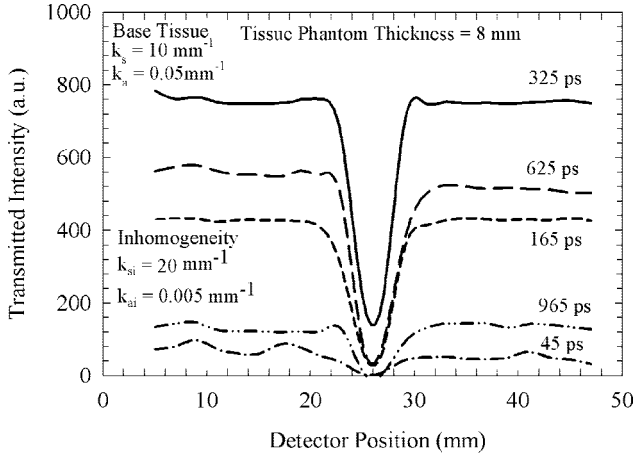

Fig. 5. Spatial transmitted intensity distribution for a tissue phantom containing an inhomogeneity at different time instants.

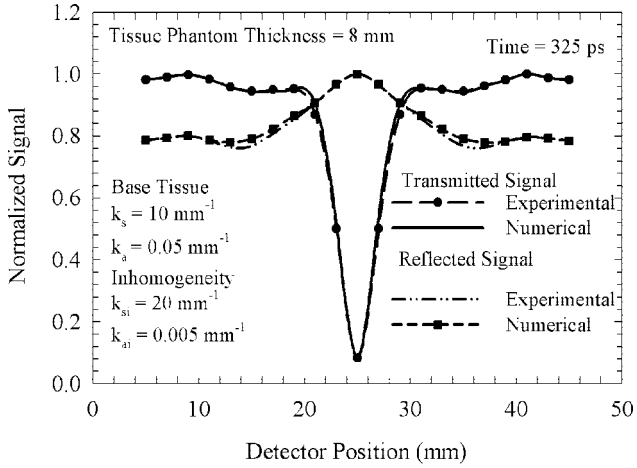

Fig. 7. Spatial transmitted and reflected signals for a tissue phantom containing an inhomogeneity at the time instant with the best contrast.

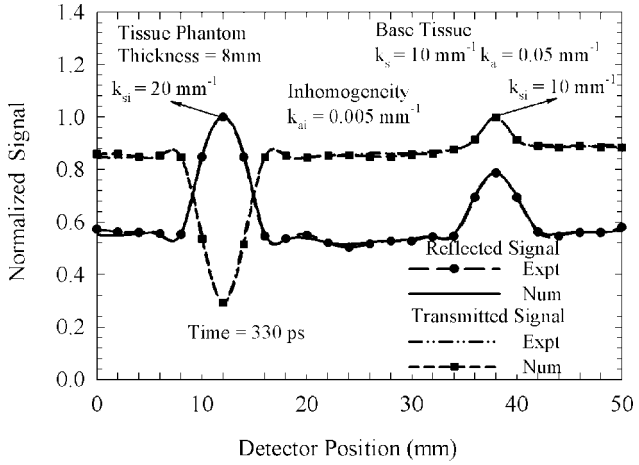

Fig. 8. Comparison between spatial transmitted and reflected signals for a tissue phantom containing two inhomogeneities at the best time instant.

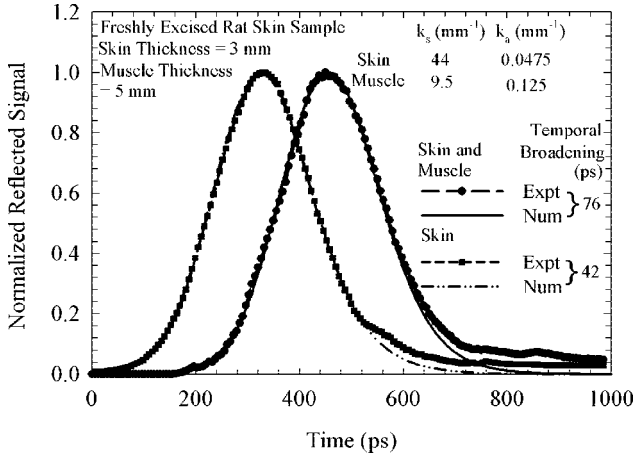

Fig. 9. Temporal reflected signals for freshly excised rat tissue samples.

base tissue, a larger number of incident photons get scattered and come back to the detector compared to those from the homogeneous base tissue region during the reflection measurement. Hence the spatial reflected signal shows a peak at the inhomogeneity location. As a large number of photons gets scattered, only a few photons penetrate the phantom thickness and reach the detector during the transmission measurement compared to the measurement from the base tissue region. This results in a deep trough in the spatial profile of the transmitted signal at the inhomogeneity site.

Figure 8 shows the comparison of the reflected and the transmitted intensities for the case of a tissue phantom containing two inhomogeneities. For this case, two inhomogeneities of 4 mm are drilled inside the tissue phantom equidistant from the central axis. The scattering coefficients of the two inhomogeneities (k_{si}) are 20 and 10 mm^{-1}, whereas the absorption coefficient (k_{ai}) is kept the same and equal to 0.005 mm^{-1}. The results are presented for 330 ps as the time instant selected corresponds to the best contrast between the tissue phantom and the inhomogeneity. Experiments are also performed at other times but have not been presented here for the sake of brevity. Since the first inhomogeneity has a higher scattering coefficient compared to the surrounding base tissue region, a greater number of photons are reflected back to the detector, and hence the reflected intensity at the first inhomogeneity location is higher in magnitude. At the same time, a decrease in the transmitted signal occurs at the first inhomogeneity location as only a few photons penetrate the phantom thickness and reach the detector. As the second inhomogeneity has the same scattering coefficient but a lower absorption coefficient compared to the base tissue, less number of photons are absorbed at this inhomogeneity location, and a considerable number of photons reach the detector during both reflection and transmission measurements resulting in an increase in signal magnitude for both cases.

B. *In Vitro* Experiments on Tissue Samples and Numerical Model Validation

An analysis of the laser-tissue interaction characteristics is necessary to obtain information about the variation of the tissue optical properties with depth. The variation of the tissue optical properties in different tissue layers can be used to monitor the progression of diseases by measuring the signal origin and the intensity. Therefore as a first step it is necessary to analyze laser interaction with healthy tissue layers to calibrate the system parameters. Tissue can be modeled primarily as having two main layers: epithelium composed of several layers of epithelial cells and stroma consisting mostly of extracellular matrix proteins and blood vessels. Therefore once the time-resolved optical detection scheme has been optimized with experiments on tissue phantoms, *in vitro* experiments are next performed on freshly excised rat tissue samples to characterize the optical signatures from these samples. Temporal optical signatures from rat skin and muscle samples are compared with the numerical modeling results. Figure 9

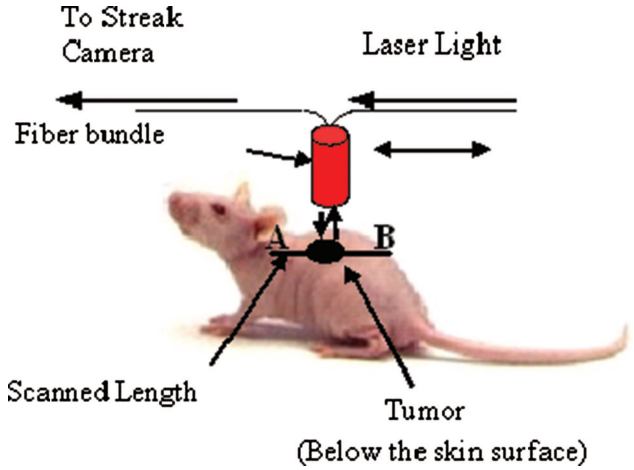

Fig. 10. (Color online) Schematic of the scanning location of an anesthetized rat injected with a tumor-promoting agent.

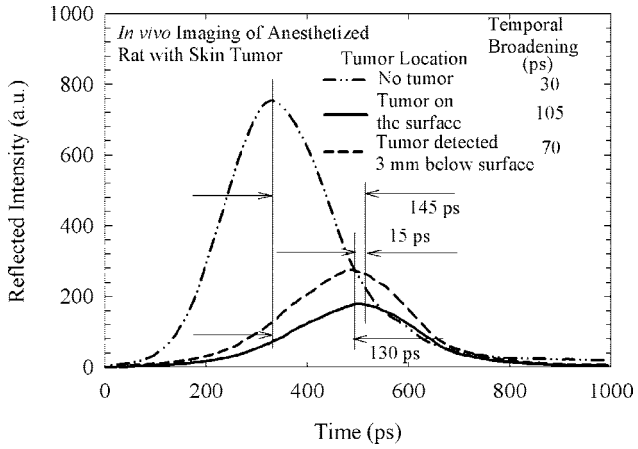

Fig. 11. Temporal reflected intensities for different tumor locations in an anesthetized rat.

shows the normalized reflected signals for the freshly excised rat skin sample and as well the rat skin and muscle combined sample. The optical properties of the rat skin and muscle are obtained from the literature.[66,67] The skin and muscle combined sample is thicker as compared to a skin-only sample. As a result, the photons encounter more multiple scattering reaching the detector while traveling through the combined skin and muscle sample than through the skin sample. This results in a higher temporal broadening of the reflected optical signals from the skin and muscle combined compared to the reflected optical signals from the skin only sample for the same incident power. The random scattering inside the muscle causes a diffuse spreading of light over a large volume. Greater optical thickness also results in a greater attenuation of the incident light.

C. Experiments on Rats with Injection of Tumor-Promoting Agents

The next step is to conduct experiments on anesthetized rats with tumor-promoting agents applied on the skin surface as well as injected below the skin

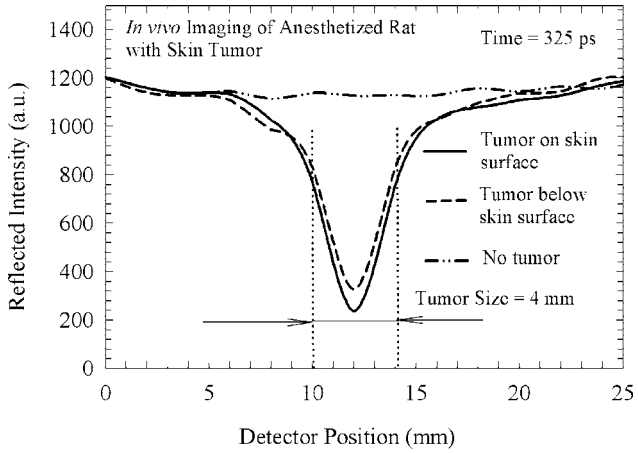

Fig. 12. Spatial reflected intensities for different tumor locations in an anesthetized rat.

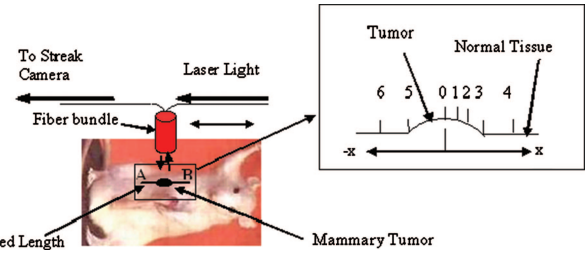

Fig. 13. (Color online) Schematic of scanning locations on an anesthetized mouse with a mammary tumor.

surface. For the case of tumor-promoting agents injected below the skin surface, the depth of the tumor from the surface is unknown, and the goal is to detect the exact location and depth of the tumor from the surface using time-resolved measurement techniques. A schematic of the rat with a tumor location is shown in Fig. 10. Figure 11 gives us a quantitative idea about the depth at which the tumor is located below the skin surface. It is observed from Fig. 11 that the reflected intensity has the highest magnitude for a rat with no tumor-promoting agent injected, since the tumor has a higher absorption than the healthy tissue. Therefore the reflected signal is significantly attenuated for the case of the tumor-promoting agent applied on the skin surface and injected below the skin surface. The key feature in this figure is the peak separation of 15 ps between the reflected signals from the tumor located below the skin and from the tumor located on the skin surface. The additional time taken by the reflected photons from the tumor on the surface to reach the detector compared to the photons reflected from the tumor located below the skin surface is 15 ps. With the tumor-promoting agent on the skin surface, the majority of the photons are absorbed and very few are reflected, while for the tumor-promoting materials injected below the skin surface, more photons are reflected from the skin surface and relatively few

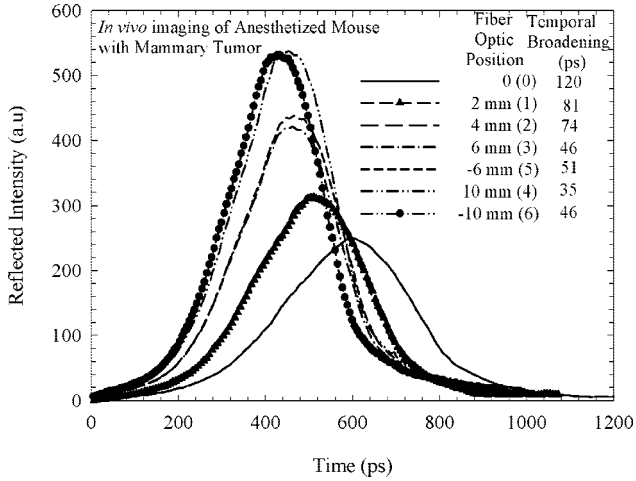

Fig. 14. Temporal reflected signals at different fiber-optic probe positions with respect to the mammary tumor location in anesthetized mice.

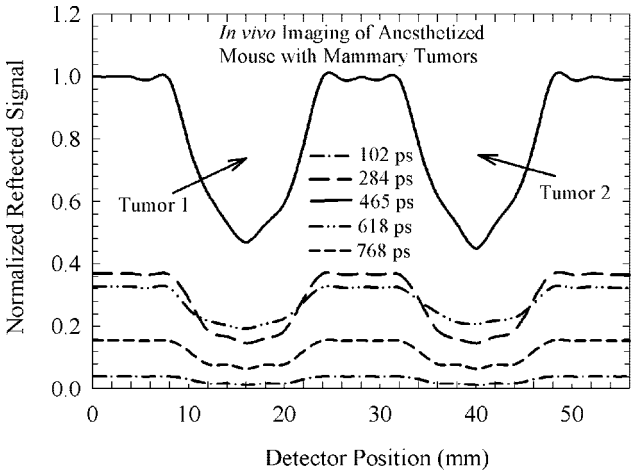

Fig. 15. Spatial reflected signals at different time instants for a mouse with two mammary tumors.

photons reach the tumor location. Multiplying the peak separation time between the reflected signals for the two cases by the speed of light in tissues (3×10^8 m/s/1.54 = 1.95×10^8 m/s) gives the depth of the tumor as 15 ps $\times$ 1.95×10^8 m/s = 2.95 mm. Thus by using this technique, a quantitative idea about the depth at which tumors are located below the skin surface can be obtained. The exact size of the tumor and also the tumor location can be obtained from the spatial profiles of the reflected optical signals by scanning over a length *AB* as shown in Fig. 10. Figure 12 shows the spatial profiles of the reflected intensity at a particular time for the tumor-promoting agents applied to the surface and as well as injected below the surface of the skin. It is observed that the reflected signals have the lowest intensity magnitude at the location of the tumor, while it increases away from the tumor site. Since tumors have a higher absorption coefficient due to an increased blood supply, it results in more absorption of photons at the tumor site compared to the surrounding healthy tissue. Therefore a reduction of the reflected intensity magnitude is observed at the tumor location.

D. Experiments on Mice with Mammary Tumors

Finally, experiments are performed on mice, with one or multiple mammary tumors; the mice are purchased from Jackson Laboratories. An area on and around both sides of the mammary tumor is scanned as shown in Fig. 13, and the scattered reflected optical signals are collected at a regular finite interval of 0.05 mm. Figure 14 shows the comparison of the reflected optical signals at different fiber-optic probe positions with respect to the tumor location. The fiber probe is scanned over a total length *AB*, and the scattered reflected signals are measured at specific points on both sides of the tumor as shown in Fig. 13 using a three-axis motorized translational stage connected to a computerized data acquisition system. It is observed that the reflected intensity is lowest in magnitude at point 0, which is the location of the tumor because tumors have higher absorbing coefficients than the surrounding healthy tissue due to increased blood flow. The magnitude of the reflected intensity increases as one moves further away from the tumor center as clearly evident from Fig. 14. Figure 15 shows the spatial profiles of the reflected intensity at different times for a mouse with two mammary tumors. As demonstrated in Subsection 5.A. in the phantom studies that the location of the tumor is best manifested within a certain time window; for this case, it corresponds to approximately 465 ps. For very short and long times, the demarcation between the tumor site and the surrounding

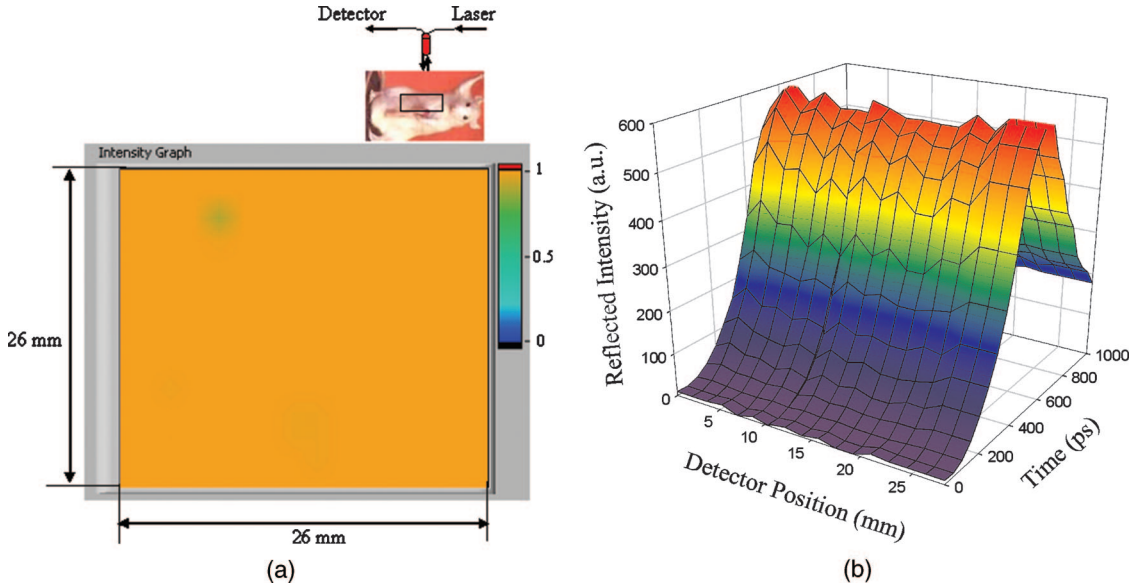

Fig. 16. (Color online) (a) Pixel representation of reflected signals for an anesthetized healthy mouse without a tumor. (b) 3D distribution of the reflected intensity for an anesthetized healthy mouse without a tumor.

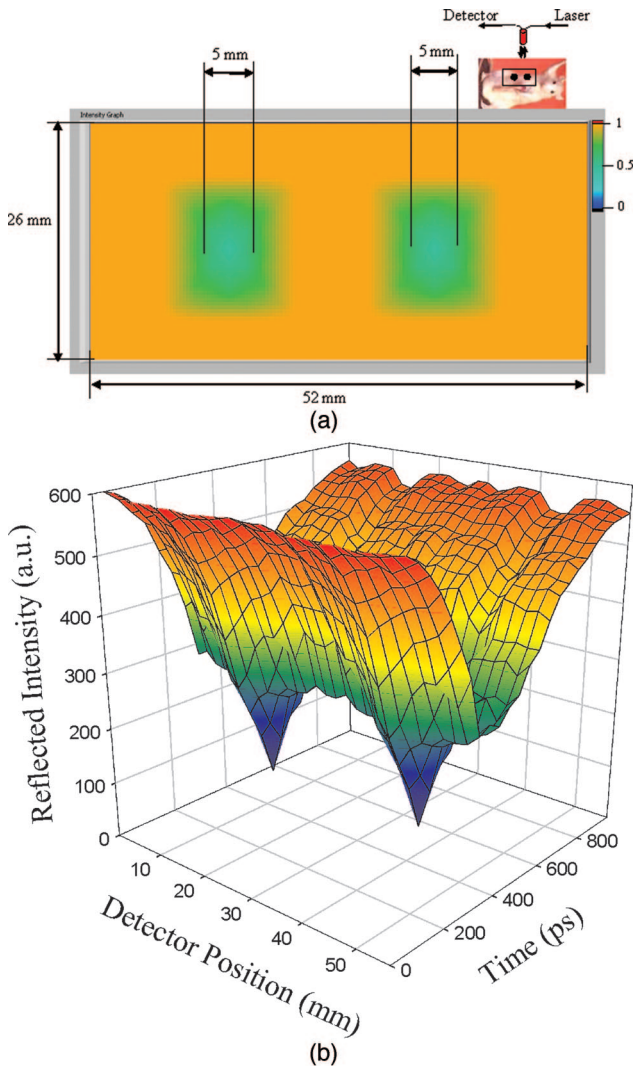

Fig. 17. (Color online) (a) Pixel representation of the reflected signals for an anesthetized mouse with two mammary tumors. (b) 3D distribution of the reflected intensity for an anesthetized mouse with two mammary tumors.

healthy tissue is not very well pronounced as evident from Fig. 15.

A better understanding of the tumor size and location can be visualized by the pixel representation of the reflected intensities as shown in Fig. 16(a) (for the case of a mouse with no tumor) and in Fig. 17(a) (for the case of a mouse with two tumors). The reflected intensities are normalized with respect to their peak values, and a pixel distribution of the intensities is obtained on a scale from 0 to 1. A pixel value of 0 implies that the entire incident light is absorbed, while a pixel value of 1 implies that the entire incident light is reflected. In this pixel representation, linear interpolation of pixel values has been performed between any two pixels using a LABVIEW image processing program. The size of the tumors is 5 mm each as actually measured and is shown in Fig. 17(a). It is also observed that there exists a transition zone between the normal tissue region and the tumor region. The corresponding 3D distribution showing the variation of the reflected intensity with space and time for both cases is presented in Figs. 16(b) and 17(b), which demonstrate the efficacy of the time-resolved optical tomography system for tumor detection in an animal model.

6. Conclusion

In this work, an extensive analysis has been performed to investigate the interaction of light with tissues with the goal of tumor detection. The experimental measurements for the case of various types of tissue phantoms and freshly excised tissue samples are in excellent agreement with the numerical modeling results. By the parametric variation of the scattering and absorption properties of the embedded inhomogeneity inside the tissue phantom, it is possible to characterize the propagation of light under various structural and physiological conditions of tissues and extract pertinent information about them. Temporal profiles of the optical signals help in providing information about the tissue optical properties, while the spatial profile at a particular time window helps in locating the tumor and/or the inhomogeneity location. In the time-resolved detection technique, the selection of an appropriate time window is critical for identifying the inhomogeneity embedded inside the tissue medium. It is observed from the time-resolved optical signal measurements in rats that one can predict the precise size, location of the tumor, and also the depth at which the tumor is located below the skin surface. This technique is also found to provide a higher-contrast image quality than the conventional imaging techniques. Results obtained from the experiments performed on a live anesthetized mouse with mammary tumors demonstrate that the time-resolved optical tomography system developed for the study of tumor detection is a clear promising alternative technique for minimally invasive diagnostics. The temporal and spatial signature of measured, transmitted, and reflected signals is able to provide a difference in the optical characteristics of the tumor region compared to the surrounding healthy tissue region from which a high-contrast image reconstruction of the interior of the tissues containing subsurface tumors is possible. Hence time-resolved optical tomography can be developed for the potential use in real-time medical diagnostics. This research can be furthered to detect tumors using the technique in organs located deep inside the body, such as the lungs, by inserting a specially designed fiber-optic probe assembly in the biopsy channel of a bronchoscope during a routine analysis.

K. Mitra acknowledges partial support from the Oak Ridge National Laboratory through contract 4000004751. T. Vo-Dinh acknowledges support from NIH grant 1 R01 CA88787-01 and the U.S. Department of Energy, Office of Environmental and Biological Research under contract DE-AC05-00OR22725 with UT Battelle, LLC.

References

1. S. Andersson-Engels, C. Klintenberg, K. Svanberg, and S. Svanberg, "*In vivo* fluorescence imaging for tissue diagnostics," Phys. Med. Biol. **42,** 815–818 (1997).
2. R. Richards-Kortum and E. Sevick-Muraca, "Quantitative optical spectroscopy for tissue diagnostics," Annu. Rev. Phys. Chem. **47,** 555–559 (1996).
3. M. Zellweger, P. Grosjean, D. Goujon, P. Monnier, and G. Wagnieres, "*In vivo* autofluorescence spectroscopy of human bronchial tissue to optimize the detection and imaging of early cancers," J. Biomed. Opt. **6,** 41–51 (2001).
4. R. R. Alfano and S. Demos, "Advances in optical biopsy and optical mammography," Ann. NY Acad. Sci. **838,** 248–270 (1997).
5. T. Vo-Dinh and P. N. Mathur, "Optical diagnostic and therapeutic technologies in pulmonary medcine," in *Interventional Bronchoscopy,* C. T. Bolliger and P. N. Mathur, eds., Prog. Respir. Res. Basel Karger **30,** 267–279 (1999).
6. R. M. Cothren, R. Richards-Kortum, M. V. Sivak, M. Fitzmaurice, R. P. Rava, G. A. Boyce, M. Doxtader, R. Blackman, T. B. Ivanc, G. B. Hayes, M. S. Feld, and R. E. Petras, "Gastrointestinal tissue diagnosis by laser-induced fluorescence spectroscopy at endoscopy," Gastroint. Endosc. **36,** 105–111 (1990).
7. R. R. Alfano, G. C. Tang, A. Pradhan, W. Lam, D. S. J. Choy, and E. Opher, "Fluorescence spectra from cancerous and normal human breast and lung tissues," IEEE J. Quantum Electron. **QE23,** 1806–1811 (1987).
8. G. C. Tang, A. Pradhan, W. Sha, J. Chen, C. H. Liu, S. J. Wahl, and R. R. Alfano, "Pulsed and cw laser fluorescence spectra from cancerous, normal, and chemically treated normal human breast and lung tissues," Appl. Opt. **28,** 2337–2342 (1989).
9. C. R. Kapadia, F. W. Cutruzzola, K. M. O'Brien, M. L. Stetz, R. Enriquez, and L. I. Deckelbaum, "Laser-induced fluorescence spectroscopy of human colonic mucosa-detection of adenomatous transformation," Gastroenterology **99,** 150–157 (1990).
10. R. Richards-Kortum, R. P. Rava, R. E. Petras, M. Fitzmaurice, M. Sivak, and M. S. Feld, "Spectroscopic diagnosis of colonic dysplacia," Photochem. Photobiol. **10,** 15–21 (1992).
11. K. T. Schomacker, J. K. Frisoli, C. C. Compton, T. J. Flotee, J. M. Richter, N. S. Nishioka, and T. F. Deutsch, "Ultraviolet laser-induced fluorescence of colonic tissue: basic biology and diagnostic potential," Lasers Surg. Med. **12,** 63–78 (1992).
12. T. Vo-Dinh, *Biomedical Photonics Handbook* (CRC, 2003).
13. J. R. Singer, F. A. Grunbaum, P. Kohn, and J. P. Zubelli, "Image reconstruction of the interior of bodies that diffuse radiation," Science **248,** 990–993 (1990).
14. B. Chance and A. Katzir, eds., "*Time-Resolved Spectroscopy and Imaging of Tissue,*" Proc. SPIE **1431** (1991).
15. F. Liu, K. M. Yoo, and R. R. Alfano, "Ultrafast laser-pulse transmission and imaging through biological tissue," Appl. Opt. **32,** 554–558 (1993).
16. S. Proskurin, Y. Yamada, and Y. Takahashi, "Absorption coefficient measurements of strongly scattering media using time-resolved transmittance of a short pulse in near-infrared wavelength range," Opt. Rev. **2,** 292–297 (1995).
17. O. Minet, G. Muller, and J. Beuthan, *Selected Papers on Optical Tomography, Fundamentals and Applications* (SPIE, 1998).
18. A. Gandjbakhche, V. Chernomordik, J. C. Hebden, and R. Nossal, "Time-dependent contrast functions for quantitative imaging in time-resolved transillumination experiments," Appl. Opt. **37,** 1973–1981 (1998).
19. V. Tuchin, *Tissue Optics* (SPIE, 2000).
20. J. C. Hebden, S. R. Arridge, and D. T. Delpy, "Optical imaging in medicine: I. Experimental techniques," Phys. Med. Biol. **42,** 825–840 (1997).
21. S. R. Arridge and J. C. Hebden, "Optical imaging in medicine: II. Modeling and reconstruction," Phys. Med. Biol. **42,** 841–853 (1997).
22. S. K. Gayen and R. R. Alfano, "Sensing lesions in tissues with light," Opt. Express **4,** 475–480 (1999).
23. H. Jiang, K. D. Paulsen, U. L. Osterberg, B. W. Pogue, and M. S. Patterson, "Simultaneous reconstruction of optical absorption and scattering maps in turbid media from near-infrared frequency-domain data," Opt. Lett. **20,** 2128–2130 (1995).
24. E. Gratton, W. M. Mantulin, M. J. vande Ven, J. B. Fishkin, M. B. Maris, and B. Chance, "A novel approach to laser tomography," Bioimaging **1,** 40–46 (1993).
25. K. W. Berndt and J. R. Lakowicz, "Detection and localization of absorbers in scattering media using frequency domain principles," in *Time-Resolved Spectroscopy and Imaging of Tissue,* B. Chance and A. Katzis, eds., Proc. SPIE **1431,** 149–160 (1991).
26. M. A. O'Leary, D. A. Boas, B. Chance, and A. G. Yodh, "Experimental images of heterogeneous turbid media by frequency domain diffusing photon tomography," Opt. Lett. **20,** 426–428 (1995).
27. Y. Yamada, "Light-tissue interaction and optical imaging in biomedicine," Ann. Rev. Fluid Mech. Heat Transfer **6,** 1–59 (1995).
28. S. Kumar, K. Mitra, and Y. Yamada, "Hyperbolic damped-wave models for transient light-pulse propagation in scattering media," Appl. Opt. **35,** 3372–3378 (1996).
29. K. M. Yoo, F. Liu, and R. R. Alfano, "When does the diffusion approximation fail to describe the photon transport in random media," Phys. Rev. Lett. **65,** 2647–2650 (1990).
30. G. Mitic, J. Kolzer, J. Otto, E. Plies, G. Solkner, and W. Zinth, "Time-gated transillumination of biological tissues and tissue like phantoms," Appl. Opt. **33,** 6699–6710 (1994).
31. R. Berg, S. Andersson-Engels, O. Jarlman, and S. Svanberg, "Time-gated viewing studies on tissue-like phantoms," Appl. Opt. **35,** 3432–3440 (1996).
32. L. Wang, X. Liang, P. A. Galland, P. P. Ho, and R. R. Alfano, "Detection of objects hidden in highly scattering media using time-gated imaging methods," in *Optical Sensing, Imaging, and Manipulation for Biological and Biomedical Applications,* R. Alfano, P. Ho, and A. Chiou, eds., Proc. SPIE **4082,** 261–264 (2000).
33. D. K. Rao, H. S. Patel, B. Jain, and P. K. Gupta, "Time-gated optical imaging through turbid media using stimulated Raman scattering: studies on image contrast," Pramana J. Phys. **64,** 229–238 (2005).
34. D. J. Hall, J. C. Hebden, and D. T. Deply, "Imaging very-low-contrast objects in breastlike scattering media with a time-resolved method," Appl. Opt. **36,** 7270–7276 (1997).
35. J. C. Hebden, "Imaging through scattering media using characteristics of the temporal distribution of transmitted laser pulses," Opt. Laser Technol. **27,** 263–268 (1995).
36. M. Q. Brewster and Y. Yamada, "Optical properties of thick, turbid media from picosecond time-resolved light scattering measurements," Int. J. Heat Mass Transfer **38,** 2569–2581 (1995).
37. W. Becker, A. Bergmann, H. Wabnitz, D. Grosenick, and A. Liebert, "High count rate multichannel TCSPC for optical tomography," in *Photon Migration, Optical Coherence, Tomography, and Microscopy,* S. Andersson-Engels and M. Kaschke, eds., Proc. SPIE **4431,** 249–254 (2001).
38. E. M. C. Hillman, J. C. Hebden, M. Schweiger, H. Dehghani, F. E. W. Schmidt, D. T. Delpy, and S. A. Arridge, "Time resolved optical tomography of the human forearm," Phys. Med. Biol. **46,** 1117–1130 (2001).
39. C. D'Andrea, D. Comelli, A. Pifferi, A. Toricelli, G. Valentini, and R. Cubeddu, "Time-resolved optical imaging through turbid media using a fast data acquisition system based on a gated CCD camera," J. Phys. D **36,** 1675–1681 (2003).
40. C. Das, A. Trivedi, K. Mitra, and T. Vo-Dinh, "Experimental and numerical analysis of short-pulse laser interaction with

tissue phantoms containing inhomogeneities," Appl. Opt. **42,** 5173–5180 (2003).
41. M. S. Patterson, B. Chance, and B. C. Wilson, "Time resolved reflectance and transmittance for the non-invasive measurement of tissue optical properties," Appl. Opt. **28,** 2331–2336 (1989).
42. A. Ishimaru, Y. Kuga, R. L. T. Cheung, and K. Shimizu, "Scattering and diffusion of a beam wave in randomly distributed scatterers," J. Opt. Soc. Am. **73,** 131–136 (1983).
43. A. H. Heelscher, S. L. Jacques, L. Wang, and F. K. Tittel, "Influence of boundary conditions on the accuracy of diffusion theory in time-resolved reflectance spectroscopy of biological tissues," Phys. Med. Biol. **40,** 1957–1975 (1995).
44. B. Chen, K. Stamnes, and J. J. Stamnes, "Validity of the diffusion approximation in bio-optical imaging," Appl. Opt. **40,** 6356–6366 (2001).
45. K. Mitra and S. Kumar, "Development and comparison of models for light pulse transport through scattering absorbing media," Appl. Opt. **38,** 188–196 (1999).
46. M. Sakami, K. Mitra, and P. Hsu, "Analysis of light-pulse transport through two-dimensional scattering-absorbing media," J. Quant. Spectrosc. Radiat. Transf. **73,** 169–179 (2002).
47. Z. Guo and S. Kumar, "Discrete-ordinates solution of short-pulsed laser transport in two-dimensional turbid media," Appl. Opt. **40,** 3156–3163 (2001).
48. A. Sawetprawichkul, P. Hsu, K. Mitra, and M. Sakami, "A Monte Carlo study of the transient radiative transfer within the one-dimensional multi-layered slab," presented at the ASME International Mechanical Engineering Congress and Exposition, Orlando, Florida, 5–10 November 2000.
49. A. Sawetprawichkul, P. Hsu, and K. Mitra, "Parallel computing of three-dimensional Monte Carlo simulation of transient radiative transfer in participating media," presented at the 8th AIAA–ASME Thermophysics and Heat Transfer Conference, St. Louis, Missouri, June 2002.
50. X. Lu and P. F. Hsu, "Reverse Monte Carlo simulations of light pulse propagation in nonhomogeneous media," J. Quant. Spectrosc. Radiat. Transf. **93,** 349–368 (2005).
51. C. Y. Wu and S. H. Wu, "Integral equation formulation for transient radiative transfer in an anisotropically scattering medium," Int. J. Heat Mass Transfer **43,** 2009–2020 (2000).
52. Z. M. Tan and P. F. Hsu, "An integral formulation of transient radiative transfer," ASME J. Heat Transfer **123,** 466–475 (2001).
53. Z. Guo and S. Kumar, "Radiation element method for transient hyperbolic radiative transfer in plane-parallel in homogenous media," Numer. Heat Transfer, Part B **39,** 371–387 (2001).
54. P. Rath, S. C. Mishra, P. Mahanta, U. K. Saha, and K. Mitra, "Discrete transfer method applied to transient radiative transfer problems in participating medium," Num. Heat Transfer, Part A **44,** 183–197 (2003).
55. S. Arride, J. Hebden, M. Schweiger, F. Schmidt, M. Fry, E. Hillman, H. Dehghani, and D. T. Delpy, "A method for three-dimensional time-resolved optical tomography," Int. J. Imaging Sys. Technol. **11,** 2–11 (2000).
56. J. M. Tualle, E. Tinet, and S. Avrillier, "New and easy way to perform time-resolved measurements of the light scattered by a turbid medium," Opt. Commun. **189,** 211–220 (2001).
57. Z. Guo, J. Aber, B. A. Garetz, and S. Kumar, "Monte Carlo simulation and experiments of pulsed radiative transfer," J. Quant. Spectrosc. Radiat. Transf. **73,** 159–168 (2002).
58. R. Cubeddu, A. Pifferi, P. Taroni, A. Torricelli, and G. Valentini, "Imaging of optical inhomogeneities in highly diffusive media: discrimination between scattering and absorption contribution," Appl. Phys. Lett. **69,** 4162–4164 (1996).
59. A. A. Lacy, T. Collier, J. E. Price, S. Dharmawardhane, and R. Richards-Kortum, "Near real-time *in vivo* confocal imaging of mouse mammary tumors," Front. Biosci. **7,** 137–145 (2002).
60. P. D. Acton and H. F. Kung, "Small animal imaging with high resolution single photon emission tomography," Nucl. Med. Biol. **30,** 889–895 (2003).
61. M. R. Rajeswari, A. Jain, A. Sharma, D. Singh, N. R. Jagannathan, U. Sharma, and M. N. Degaonkar, "Evaluation of skin tumors by magnetic resonance imaging," Lab. Invest. **83,** 1279–1283 (2003).
62. J. Masciotti, G. Abdoulaev, J. Hur, J. Papa, J. Bae, J. Huang, D. Yamashiro, J. Kandel, and A. H. Hielscher, "Combined optical tomographic and magnetic resonance imaging of tumor bearing mice," in *Optical Tomography and Spectroscopy of Tissue VI,* B. Chance, R. Alfano, B. Tromberg, M. Tamura, and E. Sevick-Muraca, eds., Proc. SPIE **5693,** 74–81 (2005).
63. N. Ramanujam, J. Chen, K. Gossage, R. Richards-Kortum, and B. Chance, "Fast and noninvasive fluorescence imaging of biologic tissues *in vivo* using a flying-spot scanner," IEEE Trans. Biomed. Eng. **48,** 1034–1041 (2001).
64. M. Firbank and D. T. Delpy, "Design for a stable and reproducible phantom for use in near infrared imaging and spectroscopy," Phys. Med. Biol. **38,** 847–853 (1993).
65. A. J. Welch and M. J. C. Van Gemert, eds., *Optical Thermal Response of Laser-Irradiated Tissue* (Plenum, 1995).
66. W. F. Cheong, S. A. Prahl, and A. J. Welch, "A review of the optical properties of biological tissues," IEEE J. Quantum Electron. **26,** 2166–2185 (1990).
67. A. M. K. Nilsson, R. Berg, and S. Andersson-Engels, "Measurements of optical properties of tissue in conjunction with photodynamic therapy," Appl. Opt. **34,** 4609–4619 (1995).